Soft Matter

Effect of Surface Tension on Elastocapillary Wrinkling of Interfacially Adsorbed Hydrogel Microdisks with Photothermally Programmed Swelling Profiles

Journal:	*Soft Matter*
Manuscript ID	SM-ART-01-2023-000001.R1
Article Type:	Paper
Date Submitted by the Author:	17-Apr-2023
Complete List of Authors:	Kim, Ji-Won; Korea Advanced Institute of Science and Technology Chen, Chao; University of Massachusetts Amherst, Polymer Science and Engineering Kim, Hyunki; University of Massaschusetts, Polymer Science and Engineering Kim, Shin-Hyun; Korea Advanced Institute of Science and Technology, Department of Chemical and Biomolecular Engineering Hayward, Ryan; University of Colorado Boulder, Chemical and Biological Engineering

Effect of Surface Tension on Elastocapillary Wrinkling of Interfacially Adsorbed Hydrogel Disks with Photothermally Programmed Swelling Profiles

Received 00th January 20xx,
Accepted 00th January 20xx

DOI: 10.1039/x0xx00000x

Ji-Won Kim,[ac] Chao Chen,[a] Hyunki Kim,[a] Shin-Hyun Kim,[c] and Ryan C. Hayward*[ab]

In this work, we study the influence of surface tension on light-induced wrinkling of hydrogel disks containing patterned regions of photothermally-active gold nanoparticles at the air-water interface. The disks, which are initially radially stretched by the air-water surface tension, undergo wrinkling under illumination through a radially nonuniform photothermal deswelling. By tuning the surface tension of the surrounding air-water interface through variations in concentration of a poly(vinyl alcohol) surfactant, we observe a critical threshold for wrinkling, followed by a monotonic decrease in wrinkle number with decreasing surface tension. Finite element simulations performed to better understand this behavior reveal qualitatively similar trends as the experiments. The insights provided into elastocapillarity-mediated wrinkling may guide future efforts to control interfacial behaviour of reconfigurable and shape-morphing films.

Introduction

Interfacial assembly techniques offer unique possibilities for defining reconfigurable and functional two-dimensionally packed structures.[1-4] To drive assembly, particles adsorbed at the interface between two immiscible fluids should exhibit significant lateral attractions. For example, when the three-phase contact line around the adsorbed particles induces deformation of the fluid interface, strong and long-ranged capillary interactions arise between particles due to the driving force to minimize the overall area of the fluid interface.[5-8] For sufficiently small particles (with low Bond number), gravitational effects can be ignored and in the absence of other body forces or torques, the interactions between particles can be described in terms of capillary multipoles of quadrupolar or higher order.[9-11]

Many studies to date have focused on spherical particles at interfaces, which can experience attractive interactions due to variations in contact line around the particle.[9-13] However, due to their highly symmetric shapes, such interactions generally give rise to nearly isotropic interactions. Therefore, to better control the directionality of particle interactions, physical or chemical anisotropy has been introduced.[14-18] For example, chemically homogeneous ellipsoidal or elongated cylindrical particles possess attractive interparticle potential along both tip-to-tip and side-to-side direction, with different values depending on their wetting properties.[19-21] Similarly, hexagram particles with hydrophobic patches at the tips led to tip-to-tip directional assembly which yielded hexagonal lattices.[22] Such directional interactions provide far greater variety of particles arrangements beyond simple dense packings. Nevertheless, the packing is generally dictated by the pre-determined anisotropy of the particles, thereby leading to formation of a single configuration.

The introduction of stimuli-responsive elements into particles with shape-programmed capillary interactions provides additional potential for reversibly and dynamically reprogramming particle assembly.[23-25] For example, our group has exploited differential swelling of thin, interfacially-adsorbed, hydrogel disks to induce responsive directional interactions between particles at fluid interfaces.[25] Using a simple method to photocatalytically reduce gold salts to plasmonic gold nanoparticles—among the most strongly absorbing photothermal agents[26]—only within the central region of a thermally-responsive hydrogel disk, we were able to drive preferential photothermally-induced shrinkage of the central region upon illumination with visible light, thereby causing the disks to wrinkle (we note that similar patterns of photothermal ink on shape memory polymer sheets has also previously been used to drive buckling into 3D shapes.[27]) While this approach has enabled rapid, reversible, and directional assembly of particles with tunable 'valence' and interaction geometry, the question of how elasticity of the disks and surface tension interact to select the number of wrinkles in this system has remained unaddressed. However, in other contexts such as morphogenesis of wrinkling of thin plastic films[28-33] at air-water interfaces, the radial tension within the material induced by the air-water surface tension is well-established to play an important role in the wrinkling behaviour.

Thus, in the current study, we seek to better understand how the air-water surface tension influences the wrinkling of interfacially-adsorbed hydrogel disks. Surface tension is varied by introducing a controlled concentration of a polyvinyl alcohol (PVOH) surfactant. PVOH was chosen as it is a nonionic surfactant and therefore reduces the influences of electrostatic interactions with the (anionically-charged) hydrogels studied. For circular hydrogel disks at the air-water interface, there is a threshold of PVOH concentration, above which wrinkling occurs under light illumination. Beyond this threshold, as surface tension decreases, the wrinkle number (i.e., the number of wrinkles formed by a given disk) decreases. Finite element simulations show a similar trend of a threshold followed by the number of wrinkles decreasing as the surface tension is reduced. These findings provide new insight for the design of programmable and reconfigurable capillary assemblies, as well

[a] Department of Polymer Science and Engineering, University of Massachusetts Amherst, MA 01003, USA.
[b] Department of Chemical and Biological Engineering, University of Colorado Boulder, CO 80303, USA. E-mail: ryan.hayward@colorado.edu
[c] Department of Chemical and Biomolecular Engineering, Korea Advanced Institute of Science and Technology (KAIST), Daejeon 34141, Republic of Korea.
† Electronic Supplementary Information (ESI) available. See DOI: 10.1039/x0xx00000x

as for the fundamental understanding of elastocapillary phenomena.

Experimental

Fabrication of a patterned hydrogel disk with localized gold nanoparticles

We synthesized patterned hydrogel disks whose deswelling is programmed through a radially nonuniform photothermal response of the gel following the procedure of Kim, et al.[25] Photocrosslinkable copolymers were synthesized through free radical polymerization with four monomers: *N*,*N*-diethyl acrylamide (DEAM, TCI) to provide temperature responsivity, acrylic acid (AAc, Sigma Aldrich) to increase the degree of swelling, acrylamidobenzophenone (AmBP) to provide photo-crosslinking and photocatalytic reduction of gold salt, and rhodamine B methacrylate (RhBMA) to aid visualization during fabrication. Of these materials, DEAM was used after purification by basic aluminum oxide, and AAc was used as received. AmBP and RhBMA were synthesized as in Kim et al.[25] Azobisisobutyronitrile (AIBN) was used as a radical initiator. The molar feed ratios of DEAM, AAc, AmBP, and RhBMA in 1,4-dioxane at 80°C were 90.8, 2, 7, and 0.2, respectively. After a day of reaction, the resulting copolymer solution was precipitated using hexane and showed number-average molecular weight M_n = 28.9 kDa with dispersity 1.76 by using gel permeation chromatography with tetrahydrofuran as an eluent and polymethylmethacrylate as a standard polymer. A gold salt ($AuCl_3 \cdot 3H_2O$, Sigma-Aldrich) was mixed into the copolymer solution which can subsequently be photocatalytically reduced by benzophenone to form gold nanoparticles (Au NPs) selectively within illuminated regions.[34] The solution used for drop-casting was composed of 4.7 w/w% of copolymer, 0.94 w/w% of gold salt, and 0.8 v/v% of diethylene glycol (DEG, Sigma-Aldrich) in 1-propanol (anhydrous 99.7%, Sigma-Aldrich).

Prior to preparing a copolymer film, 4 w/w% of polyvinyl alcohol (PVOH, 13-23 kDa, 87% hydrolyzed, Sigma-Aldrich) aqueous solution was spun-coat on a bare silicon wafer (1 cm x 1 cm) as a sacrificial layer (5000 rpm for 60 s). We next drop-casted the copolymer solution on the sacrificial layer inside of a closed amber glass jar at a nitrogen atmosphere for at least 12 h. To adjust the thickness of the resulting film, the solution volume used for the drop-casting was controlled as 15, 30, and 45 µL leading to 2.3, 4.6, and 9.3 µm thick films, respectively, measured using an optical profilometer (Zygo NewView 7300).

We patterned the hydrogel and gold-nanoparticles selectively by controlling the dose of UV and violet radiation using a digital micromirror device (DMD, DLP Discovery 4100, Texas Instruments). A silicon wafer with spin-coated PVOH layer and drop-casted polymer film was placed face down on the stage of an inverted optical microscope (Nikon ECLIPSE Ti) and patterned by exposure for 60 s to 365 nm UV light reflected from the DMD into the microscope, with an intensity of 0.17 W/cm² at the sample plane to crosslink a circular disk of polymer with diameter L = 400 µm. The Au NPs were then formed only in a smaller concentric circular region with diameter a = 200 µm by photocatalytic reduction using 400 nm

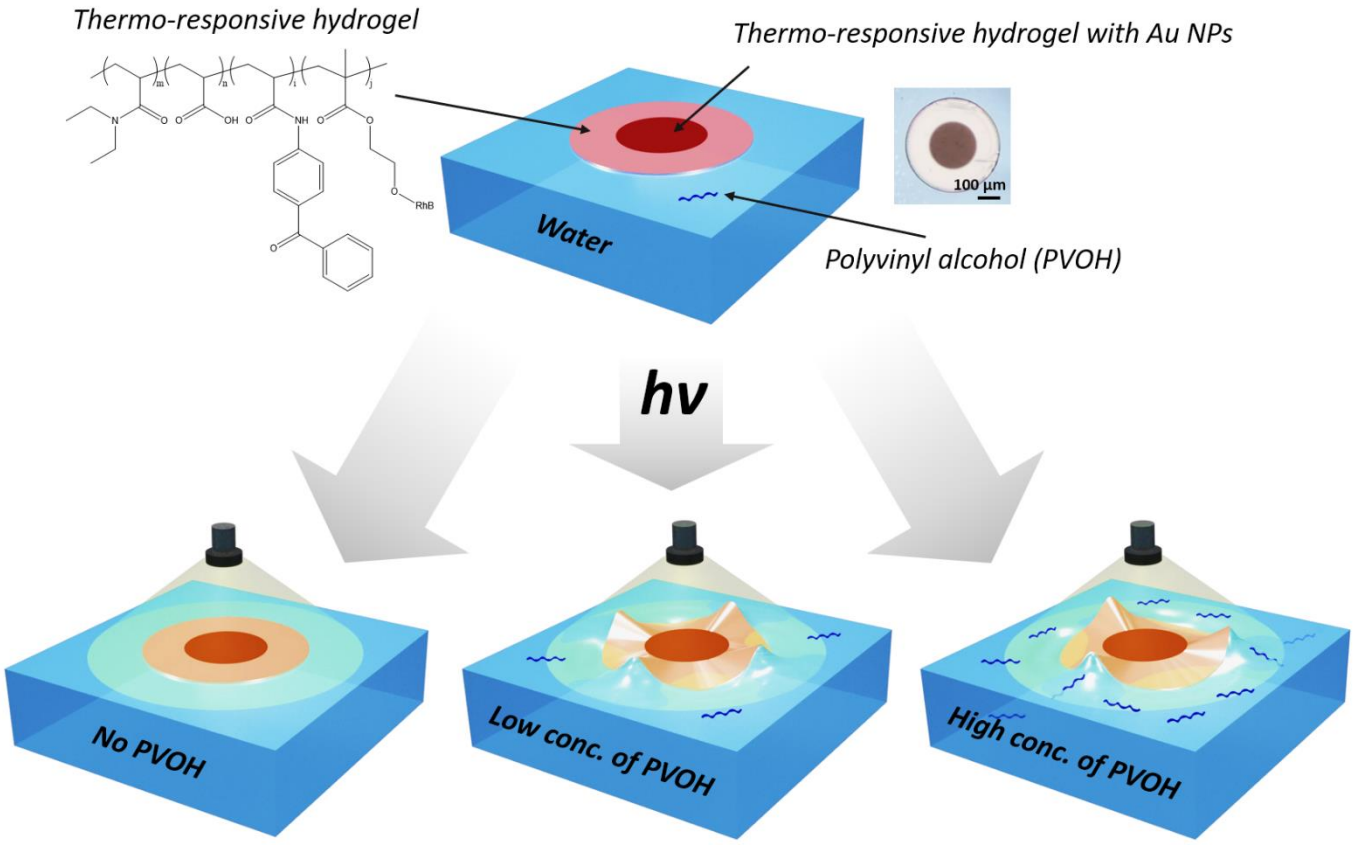

Figure 1. Schematic illustration of an interfacially adsorbed hydrogel disk with a photothermally programmed swelling profile. Light is illuminated at different polyvinyl alcohol (PVOH) aqueous solution concentrations.

of violet light with higher intensity (2.24 W/cm^2) for 800 s. After patterning both hydrogel and NPs, the uncrosslinked polymer and the residual gold salt were dissolved in a mixture of 4-methyl-2-pentanone and hexane with 17 to 3 volumetric ratio for 90 s followed by blowing dry with compressed air. The microscopic images of patterned hydrogel disks with different thicknesses are shown in Fig. S1.

The patterned disks were then released from the wafer by gently shaking the wafer inside of reverse osmosis (RO)water for 1 min. Released disks were able to be placed at the air-water interface by carefully lifting them from below using tweezers. Since the water contains an uncontrolled amount of PVOH due to the dissolution of the sacrificial layer during the releasing step, we transferred the disks, using tweezers, first to another container of pure water for washing, then to a phosphate buffered saline (PBS, Sigma-Aldrich) solution diluted 10x to yield a total buffer strength of 1 mM; this medium leads to greater swelling than in either pure water or undiluted PBS, as the acrylic acid moieties remain highly charged but their effect is not screened by too high of an ionic strength. Finally, disks were transferred to an aqueous solution containing a known concentration of PVOH as well as PBS with 1 mM buffer strength. The surface tension of the solution was adjusted by the PVOH aqueous solution concentration. We measured the

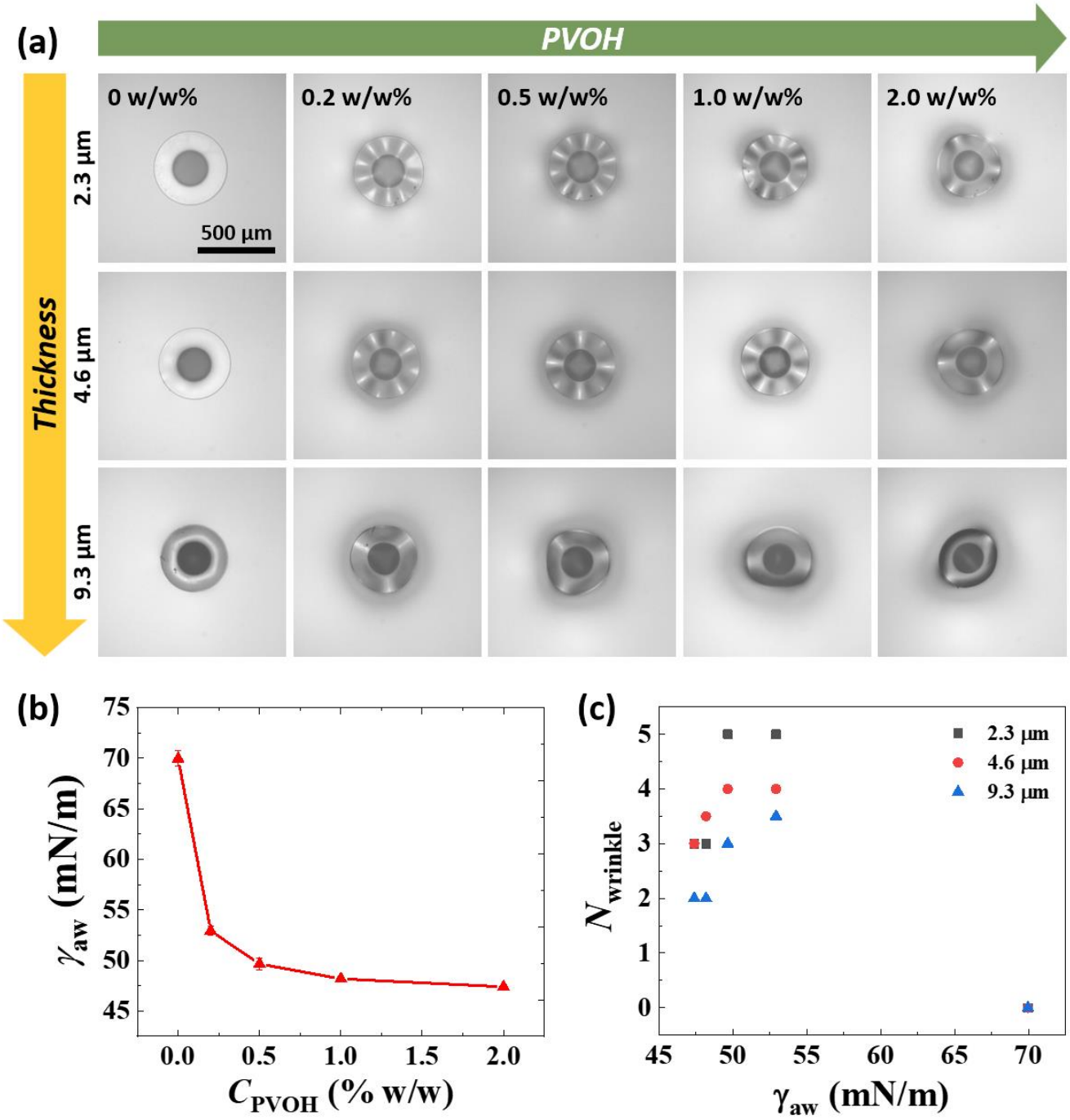

Figure 2. (a) A series of optical microscopy images of hydrogel disks with different PVOH aqueous solution concentrations and disk thicknesses. (b) A plot of surface tension of air-water interface with surfactants at different PVOH aqueous solution concentrations. (c) A plot showing how the wrinkle number depends on the air-water surface tension for three different disk thicknesses.

surface tension via the pendant drop method using an optical tensiometer (Biolin Scientific).

Finite element modeling

We employed finite element analysis using Abaqus software (Dassault Systèmes) to model the photothermal wrinkling of hydrogel disks subject to external surface tension. The disks were modeled with shell elements SR4. The dimensions of the disks were matched to the nominal (as fabricated) sizes used in experiments. The Young's modulus of the gel was set to 0.120 MPa, the value measured for experimental samples using a custom interfacial tensile tester[35], the Poisson's ratio as 0.3, a typical value for a hydrogel at equilibrium, and the linear thermo-expansion coefficient as -0.01 K^{-1}, as determined in our previous report.[25] An outward line tension was applied along the circumference of the gel to model the effect of the net surface tension. Finally, we conducted a linear perturbation simulation on the pre-tensioned disks, subject to a radial temperature profile designed to capture that experienced by the disks in experiments (Fig. S2). Upon increasing the overall magnitude of the temperature profile, we identified the first mode to become unstable in terms of the wrinkle number and the critical temperature increase needed to initiate wrinkling.

Results and discussion

The wrinkling of interfacially-adsorbed hydrogel disks shows substantial sensitivity to the presence of surfactant, as shown schematically in Fig. 1, and summarized in Fig. 2a. Specifically, we illuminated disks with white light with an intensity of 5.5 W/cm^2 for at least 10 s (a sufficient time to reach steady-state; see Movie S1) and monitored how the presence, and number, of wrinkles depended on the concentration of incompletely hydrolyzed polyvinyl alcohol (PVOH), which is well known to reduce the air-water surface tension[36]. The wrinkle number is determined by counting the number of raised 'crests', or equivalently of lowered 'troughs', by adjusting the focal plane of the optical microscope to be above or below the air-water interface, respectively. Here, we keep the light intensity fixed at 5.5 W/cm^2, leading to an estimated temperature increase of 13 K (Fig. S2), and a corresponding linear strain of – 0.13, at the centre of the disk. However, as also noted in our prior work[25], variations in light intensity led to only changes in wrinkle amplitude, not wrinkle number. As seen in Fig. 2b, the air-water surface tension γ_{aw} was progressively reduced from 70 mN/m for 1 mM phosphate buffered saline (PBS) aqueous solution to 47 mN/m for 1 mM PBS solution with 2 w/w% of PVOH. Further increases in concentration of PVOH led to the disks no longer stably adsorbing to the interface. This suggests that the interfacial driving force for adsorption of the disk, given by $\gamma_{aw} + \gamma_{gw} - \gamma_{ag}$, where γ_{gw} and γ_{ag} respectively represent the gel/water and air/gel interfacial tensions, drops to zero at just above 2 w/w% PVOH. Hence, we can estimate $\gamma_{ag} - \gamma_{gw} \approx 47$ mN/m. We note that PVOH may also adsorb to the gel/water and/or air/gel interfaces, although the driving force for either will be much weaker than to the air/water influence, and hence we neglect these possibilities in the following. Further, noting that the gel contains substantial amounts of water when

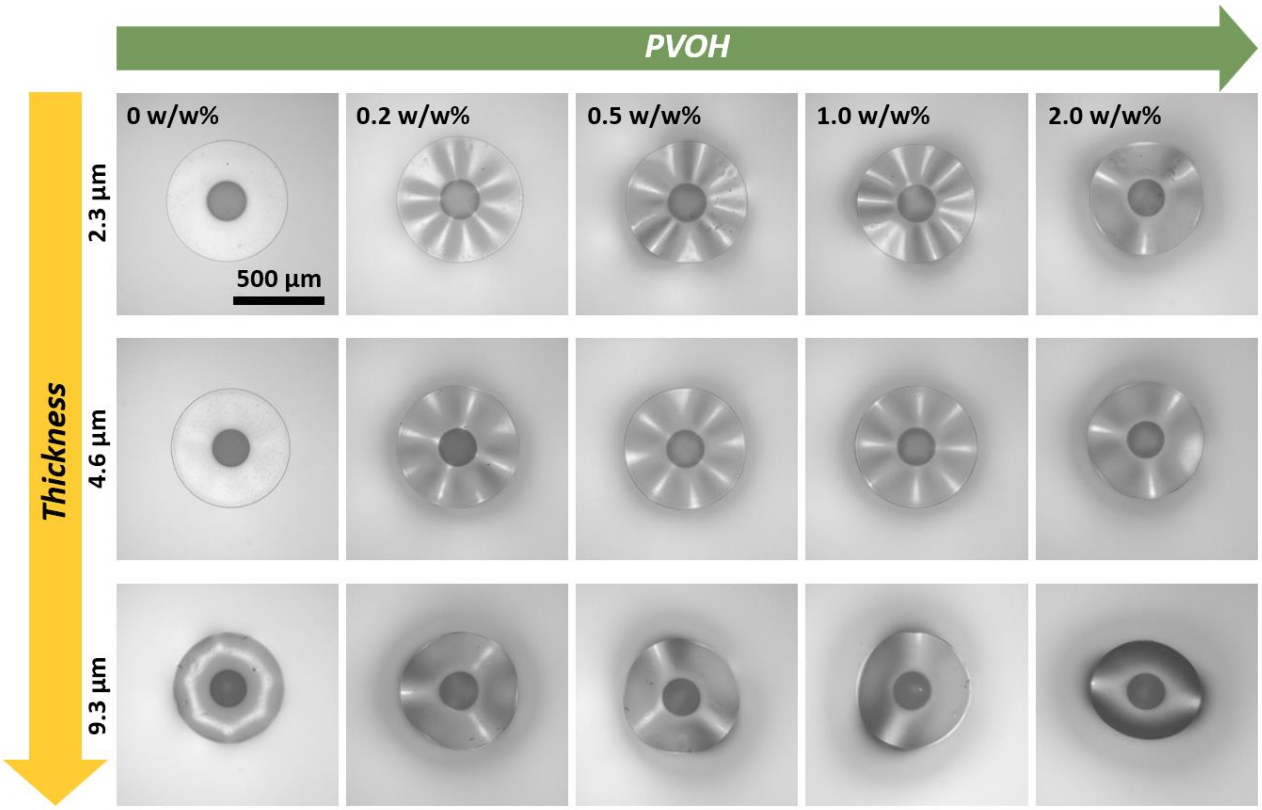

Figure 3. A series of optical microscope images of adsorbed hydrogel disks with a value of a/L = 0.33 with surfactant concentrations (left-to-right): 0%, 0.2%, 0.5%, 1.0%, 2.0% (w/w) and thicknesses (top-to-bottom): 2.3 µm, 4.6 µm, 9.3 µm.

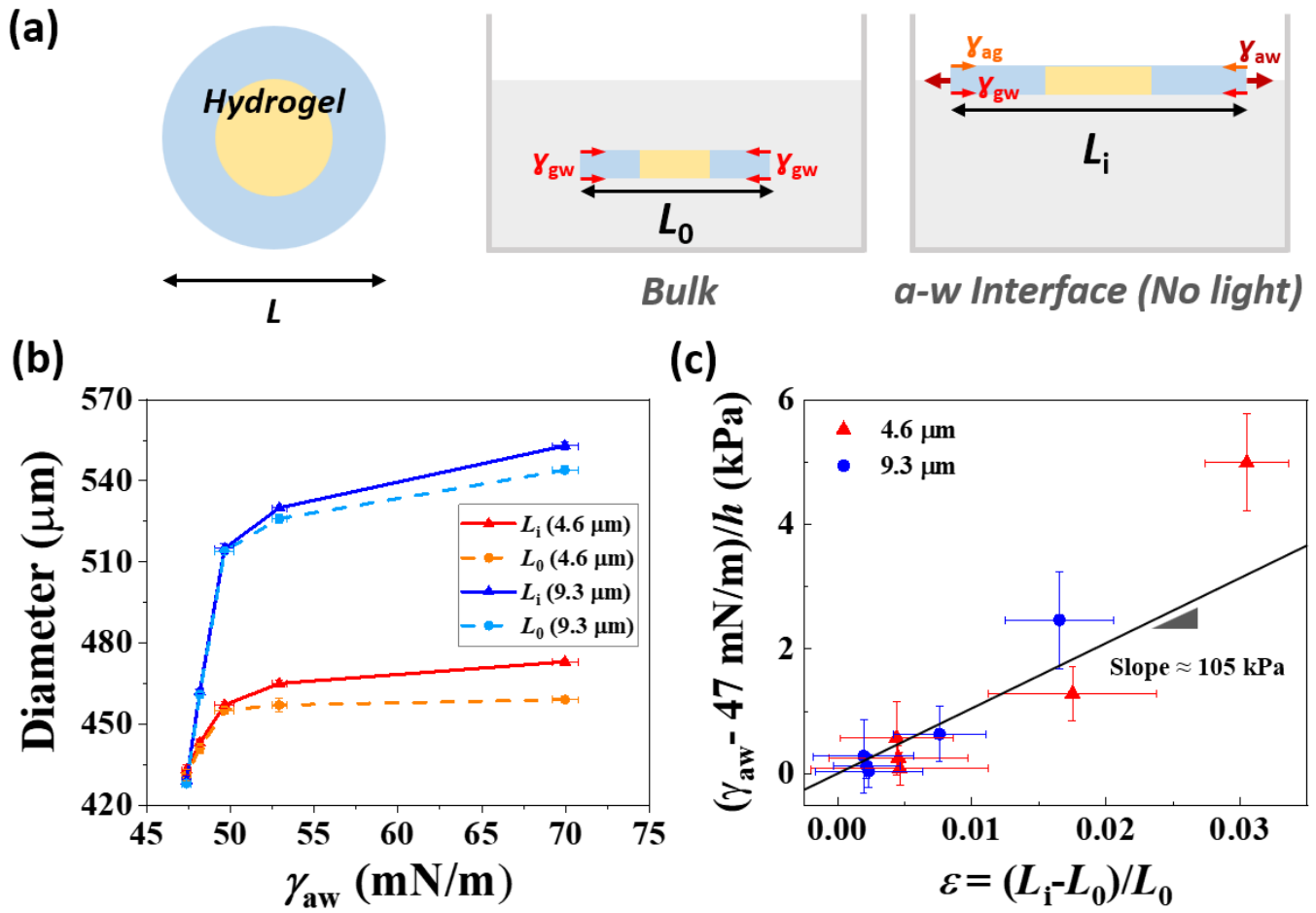

Figure 4. (a) Schematic illustration of a gold patterned hydrogel disk in two situations. One is inside of a bulk solution, and the other is adsorbed at an air-water interface (a-w interface). L0 and Li indicate the overall hydrogel diameter in these respective situations. (b) A plot of the measured hydrogel diameters in these two situations for different thicknesses and surface tensions. (c) A plot comparing the stress applied to the hydrogel disks, calculated as the net outward surface tension divided by thicknesses, to the resulting strain on the hydrogel disks, calculated from the data in (b). The solid line represents a best fit to the combined data for both thicknesses with fixed intercept (0,0).

swelled, we may estimate that γ_{gw} is likely very small compared to the other surface tensions and hence that $\gamma_{ag} \approx 47$ mN/m.

Several key results emerge from the data in Fig. 2a. First, for each thickness (2.3, 4.6, and 9.3 μm), samples remain planar under illumination at a pure water/air interface, and only undergo wrinkling for PVOH concentrations equal to or greater than 0.2 w/w%. We note that in our previous report[25], although PVOH was not intentionally added to the medium, substantial concentrations were likely present from dissolution of the sacrificial film, as we did not perform a washing step in that case. This, potentially along with the presence of other surface-active impurities from e.g., plasticware used in the experiments, likely explains why wrinkling was previously observed even at nominally 'pure' water/air interfaces. Second, beyond this threshold, samples of each thickness show a monotonic decrease in wrinkle number with increasing PVOH concentration. Finally, at any given PVOH concentration above the threshold, the number of wrinkles decreases as the film thickness is increased. The results are quantified in Fig. 2c; in most cases two or three replicate samples each showed the same number of wrinkles. However, in two cases we found one example each of consecutive integer wrinkle number; in these cases we plot the average of the two values. All three behaviours can be qualitatively understood as follows. The high surface tension of the air-water interface causes the disk to stretch radially, placing it under equibiaxial tension. Upon contraction of the central portion of the disk under illumination, the resulting azimuthal compression is partially offset by this pre-tension, which reduces the tendency for wrinkling. For a sufficiently large tension (pure water), the effect is to completely suppress wrinkling under these conditions. As surface tension is decreased below the threshold, wrinkles with higher amplitude, and therefore fewer number, become energetically less costly, since they result in lower bending energy of the disk and the penalty associated with the larger surface area is reduced. This leads to the decrease in wrinkle number as surface tension is decreased from ≈ 53 to 47 mN/m in Fig. 2c. Notably, the wrinkle number does not appear to be highly sensitive to the relative dimensions of the gold-loaded and unloaded portions of the disk, as we found that increasing the overall disk size to L = 600 μm while keeping the size of the gold-loaded portion a constant at 200 μm (i.e., a change in aspect ratio from a/L = 1/2 to 1/3) did not alter the number of wrinkles as shown in Fig. 3

To provide support for the picture described above, we first quantified the degree of stretching of the disks at the air-water

interface, as shown in Fig. 4, S3 and S4. We measured the overall hydrogel diameter while submerged in bulk aqueous solution L_0 and when adsorbed at the air-water interface L_i and then determined the magnitude of biaxial strain $\varepsilon = L_i/L_0 - 1$, as shown in Fig. 4b. Comparing these two states in Fig. 4a, we see that the radial tension applied to the interfacially adsorbed disk should be given by the spreading parameter of the gel, $S_g = \gamma_{aw} - \gamma_{gw} - \gamma_{ag}$, whereas in the bulk the disk should be compressed by an amount $2\gamma_{gw}$. Thus, we expect the increase in dimension to be governed by the difference between these two, i.e., $\gamma_{aw} + \gamma_{gw} - \gamma_{ag} \approx \gamma_{aw}$ - 47 mN/m. We first note that the gels decrease in linear swelling ratio by up to ≈ 10 – 20% upon addition of PVOH, presumably reflecting a decrease in the chemical potential of water and therefore a smaller driving force for swelling. However, upon absorption to the air-water interface, substantial stretching of disks could be observed, at least for the higher values of γ_{aw}. Since the thinnest disks with h = 2.3 μm typically became folded upon themselves within the bulk as shown in Fig. S4, we were unfortunately not able to measure their degree of stretching. To present these data in a form most comparable to a tradition stress-strain plot, we determined the stress as the net tension divided by the gel thickness (γ_{aw} - 47 mN/m)/h and plotted it against the measured strain ε, as shown in Fig. 4c (see Fig. S5 for unnormalized data). This results in a good collapse of the data for both h = 4.6 and 9.3 μm, and yields a best-fit slope of 105 kPa. This value is in reasonably good agreement with that of the biaxial modulus $Eh/(1-\nu)$ ≈ 170 kPa determined from the independently-measured value of the Young's modulus E = 0.120 MPa, and an estimated Poisson's ratio of $\nu \approx 0.3$ which is typical for a hydrogel at equilibrium. This good correspondence provides strong support for the picture described above for how the net tension biaxially stretches the disks upon adsorption at the air/water interface.

To provide further insight into the influence of surface tension on photothermal wrinkling of disks, we conducted finite element modelling (FEM) using Abaqus, as shown in Fig. 5. The numerical calculation considers the wrinkling caused by the thermal deswelling balanced with the surface tension γ which is imposed through an outward radial tension applied to the circumference of these disks. For low values of γ, the wrinkle number associated with the first unstable mode increases as the surface tension increases. Meanwhile, the threshold temperature rise necessary to trigger wrinkling also increased. Beyond critical threshold values of 2.2 mN/m for a thickness of 2.3 μm, 3.8 mN/m for a thickness of 4.6 μm, and 5.7 mN/m for a thickness of 9.3 μm, the simulation results showed no wrinkling for the value of the maximum temperature increase at the disk centre of ΔT = 13 K that is estimated to occur in the experiments.

Comparing the FEM results on wrinkle number vs. surface tension in Fig. 5b with the experimental measurements in Fig. 2c, we see that the two are in reasonably good qualitative agreement in several respects. At the lowest values of surface tension, both experiments and FEM show a small wrinkle number (2 – 3), which increases as γ is raised. Both also show a maximum number of wrinkles before reaching a threshold value of tension where wrinkling is entirely suppressed, although the simulations predict a somewhat larger maximum wrinkle number (6 – 9) for the two thinner disks), compared to the experimentally-measured values (4 – 5). This level of quantitative disagreement is reasonable considering that we have only coarse estimates for parameters such as the Poisson's ratio of the gel, and that FEM does not account for changes in

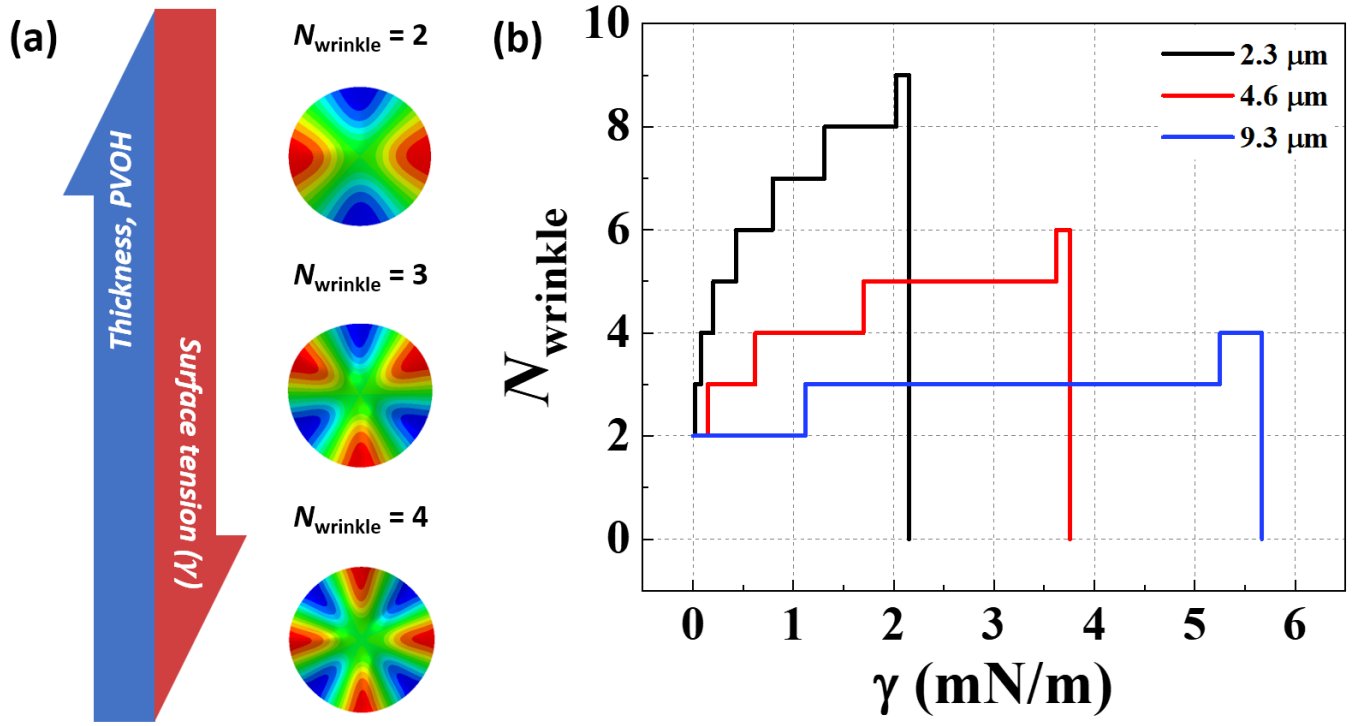

Figure 5. (a) Estimated wrinkling behaviour of hydrogel disks obtained from Abaqus simulation at low surface tension range, beyond a critical threshold. (b) The calculated number of wrinkles depend on surface tension values with gradient temperature profiles in Abaqus simulation.

gel thickness due to swelling or heating-induced deswelling, as well as associated changes in gel modulus. Notably, FEM predicts threshold values of γ = 2.2 – 5.7 mN/m, whereas the experiments show values of γ_{aw} between 55 and 70 mN/m. This would represent quite poor agreement if we tried to directly equate the two. However, if we instead compare γ to the *net* outward tension on the gel, i.e., $\gamma_{aw} - \gamma_{gw} - \gamma_{ag}$ which can be taken as approximately γ_{aw} – 47 mN/m using the estimates described above, then the experimentally measured thresholds of ≈ 8 – 23 mN/m are at least of similar magnitude to the FEM predictions. At some level, this correspondence seems natural, given that the results in Fig. 4 are consistent with a net tension of $\gamma_{aw} - \gamma_{gw} - \gamma_{ag}$ being applied to the interfacially-adsorbed disk. However, we note that Kumar, et al[32]. have suggested that interfacially-adsorbed elastic sheets should be treated as subject to the full tension γ_{aw}. In any case, it is clear that our FEM model is somewhat simplified compared to reality--for example, if we let γ_{gw} = 0, then at the point where $\gamma_{aw} = \gamma_{ag}$, our model would predict no influence of surface tension at all, whereas in reality both the air-water and air-gel interface remain under nearly equal tension. Thus, additional modelling that accounts for surface tension in a more complete way would be valuable to pursue in the future.

Conclusions

In this work, we have studied the influence of surfactant-induced reductions in surface tension on the wrinkling behaviour of gold-containing hydrogel disks subject to light. The localized patterning of gold nanoparticles in thermo-responsive hydrogels drives wrinkling of interfacially-adsorbed disks under illumination due to preferential contraction of the central region. However, the air-water surface tension is found to measurably stretch the disks, and this pre-tension is found to completely suppress wrinkling beyond a critical threshold, and subsequently modify wrinkle number in a thickness-dependent fashion. Our experimental results are in good qualitative agreement with finite element simulations, although obtaining a full quantitative understanding will likely require the development of more sophisticated approaches to incorporate surface tension into the model. In any case, our findings provide new insights into elastocapillary wrinkling phenomena as well as a facile method to tune the wrinkling behaviour of stimuli-responsive interfacially-adsorbed particles that are well-suited for studies on capillary assembly.

Conflicts of interest

There are no conflicts to declare.

Acknowledgements

The authors express their gratitude to Prof. Thomas P. Russell on the occasion of his 70th birthday for his support, mentoring, and friendship over the years, along with many engrossing scientific discussions about thin sheets at interfaces and other topics, we thank Prof. Alfred J. Crosby for the use of optical profilometer and The Uniaxial Tensile Tester for Ultrathin films (TUTTUT). This research was supported by the Army Research Office through grants W911NF-21-1-0068 and W911NF-19-1-0348. J.-W.K. was supported by the Brain Korea 21 (BK21) visiting scholar program funded by the National Research Foundation (NRF) of Korea.

References

1 M. A. Bucaro, P. R. Kolodner, J. A. Taylor, A. Sidorenko, J. Aizenberg and T. N. Krupenkin, *Langmuir,* 2009, **25**, 3876.
2 Y. Du, E. Lo, S. Ali and A. Khademhosseini, *PNAS,* 2008, **105**, 28, 9522.
3 P. Aussillous and D. Quéré, *Nature*, 2001, **411**, 924.
4 D. Suzuki, S. Tsuji and H. Kawaguchi, *J. Am. Chem. Soc.,* 2007, **129**, 8088.
5 P. A. Kralchevsky and K. Nagayama, *Adv. Colloid Interface Sci.*, 2000, **85**, 145-192.
6 L. Duan, C. Wang, W. Zhang, B. Ma, Y. Deng, W. Li, and D. Zhao, *Chem. Rev.*, 2021, **121**, 14349-14429.
7 A. C. Nickel, A. A. Rudov, I. I. Potemkin, J. J. Crassous, and W. Richtering, *Langmuir*, 2022, **38**, 4351-4363.
8 M. Cavallaro, L. Botto, E. P. Lewandowski, M. Wang, and K. J. Stebe, *PNAS*, 2011, **108**, 20923-20928.
9 R. McGorty, J. Fung, D. Kaz, V. N. Manoharan, *Materials Today,* 2010, **13**, 6, 34.
10 P. A. Kralchevsky, K. Nagayama, *Langmuir,* **1994**, *10*, 23.
11 P. A. Kralchevsky, N. D. Denkov, K. D. Danov, *Langmuir,* 2001, **17**, 7694.
12 M. Oettel, S. Dietrich, *Langmuir,* 2008, **24**, 1425.
13 A. Maestro, O. S. Deshmukh, F. Mugele, D. Langevin, *Langmuir,* 2015, **31**, 6289.
14 N. Bowden, I. S. Choi, B. A. Grzybowski, G. M. Whitesides, *J. Am. Chem. Soc.,* 1999, **121**, 23.
15 A. B. Pawar, I. Kretzschmar, *Langmuir,* 2008, **24**, 355.
16 Q. Chen, S. C. Bae, S. Granick, *Nature*, 2011, **469**, 381.
17 B. J. Park, C.-H. Choi, S.-M. Kang, K. E. Tettey, C.-S. Lee, D. Lee, *Langmuir,* 2013, **29**, 1841.
18 D. Kim, W. K. Bae, S.-H. Kim, D. C. Lee, *Nano Lett.,* 2019, **19**, 963.
19 J. C. Loudet, A. M. Alsayed, J. Zhang, A. G. Yodh, *Physical Review Letters,* 2005, **94**, 018301.
20 E. P. Lewandowski, M. Cavallaro, L. Botto, J. C. Bernate, V. Garbin, K. J. Stebe, *Langmuir*, **2010**, *26*, 15142.
21 L. Botto, L. Yao, R. L. Leheny, K. J. Stebe, *Soft Matter*, **2012**, *8*, 4971.
22 S.-M. Kang, C.-H. Choi, J. Kim. S.-J. Yeom, D. Lee, B. J. Park, C.-S. Lee, *Soft Matter*, 2016, **12**, 5847.
23 J. Bae, N. P. Bende, A. A. Evans, J.-H. Na, C. D. Santangelo, R. C. Hayward, *Mater. Horiz.,* 2017, **4**, 228.
24 W. Wang, J. Giltinan, S. Zakharchenko, M. Sitti, *Sci. Adv.,* 2017, **3**, 1602522.
25 H. Kim, J.-H. Kang, Y. Zhou, A. S. Kuenstler, Y. Kim, C. Chen, T. Emrick, R. C. Hayward, *Adv. Mater.,* 2019, **31**, 1900932.
26 H. Han, K. Choi, *Biomedicines*, 2021, **9**, 305.
27 R. W. Mailen, C. H. Wagner, R. S. Bang, M. Zikry, M. D. Dickey, J. Genzer, *Smart Mater. Struct.*, 2019, **28**, 045011.
28 J. Huang, M. Juszkiewicz, W. H. de Jeu, E. Cerda, T. Emrick, N. Menon, T. P. Russell, *Science*, **2007**, *317*, 650.
29 J. Huang, B. Davidovitch, C. D. Santangelo, T. P. Russell, N. Menon, *Physical Review Letters*, **2010**, *105*, 038302.
30 R. D. Schroll, M. Adda-Bedia, E. Cerda, J. Huang, N. Menon, T. P. Russell, K. B. Toga, D. Vella, B. Davidovitch, *Physical Review Letters*, **2013**, *111*, 014301.
31 J. Chang, K. B. Toga, J. D. Paulsen, N. Menon, T. P. Russell, *Macromolecules*, **2018**, *51*, 6764.

32 D. Kumar, T. P. Russell, B. Davidovitch, N. Menon, *Nature Materials*, **2020**, *19*, 690.
33 N. Bowden, W. T. S. Huck, K. E. Paul, G. M. Whitesides, *Appl. Phys. Lett.*, **1999**, *75*, 2557.
34 M. L. Marin, K. L. McGilvray, J. C. Scaiano, *J. Am. Chem. Soc.,* 2008, **130**, 16572.
35 R. K. Bay, A. J. Crosby, *ACS Macro Lett.,* 2019, **8**, 1080.
36 J. M. G. Lankveld, J. Lyklema, *J. Colloid Interface Sci.,* 1972, **41**, 454.